Static and Dynamic Crack Toughness of Brazed Joints of Inconel 718 Nickel-Base Alloy

The heat-treatment homogenization of brazed joints to achieve the desirable distribution of brittle phases is accompanied by measurable decreases in tensile strength and crack toughness

BY B. Z. WEISS, H. D. STEFFENS, A. H. ENGELHART AND B. WIELAGE

ABSTRACT. The crack toughness of brazed joints of Inconel 718 nickel-base alloy was investigated at different strain rates. The brazing filler metal used was BNi5. The results were compared with those obtained on specimens made of the base material. The brazed joints were heat-treated after the brazing process in order to achieve a desirable distribution of the brittle phases in the joint.

Tests for the determination of static tensile properties, carried out on five series of specimens, showed that the "post-brazing" heat treatment leads to a certain decrease in tensile strength. In the static and the quasi-dynamic crack toughness investigations, acoustic emission measurements were conducted simultaneously with load and COD measurements.

In all specimens made of the base material, no acoustic emissions could be detected. This was explained by the fact that Inconel 718 has an FCC structure in which most of the grown-in dislocations are mobile, and their motion begins with the onset of the load. In the brazed joints plastic deformation occurs under constraint conditions, leading to a relatively rapid motion of dislocations, and emissions of acoustic signals are consequently intense. In addition to acoustic emissions associated with plastic deformation, emissions resulting from crack formation and propagation in the brittle phases could be easily recorded.

In the base material fracture occurs after general yielding; the crack toughness values were, therefore, calculated by the "equivalent energy" method. The prolonged homogenization at 1100 C (2012 F) results in a decrease in the crack toughness of the base material by ~10%. In contrast to the base material the fractures of the brazed joints were of a typical brittle character, evidenced by the linear dependence between load and time. The crack toughness of the brazed joints is much lower than that of the base material. The drop is quite drastic and amounts on an average to ~80%.

Another difference observed is a certain dependence of the crack toughness of the brazed joint on the strain rate, an effect which was not observed in the base material. Fractographic investigations carried out on fractured surfaces of specimens of the base material showed that fracture occurs by microscopic plastic deformation processes, while in the brazed joint, fracture is of a cleavage or quasi-cleavage character.

B. Z. WEISS is Professor, Department of Materials Engineering, Technion-Israel Institute of Technology, Haifa, Israel; H. D. STEFFENS is a Professor, and A. H. ENGELHART and B. WIELAGE are Research Associates, Mechanical Engineering Faculty, Dortmund University, West Germany.

Introduction

Brazing has been an important and widely used joining process for several decades but has only recently assumed an increasing role in the manufacture of hardware utilized in different fields such as the automobile, aircraft, military and nuclear industries. However, the penetration of brazing into industry has been rather slow because of the severe heat and corrosion resistance requirements. In order to meet these needs, the conventional silver alloy compositions were replaced by new nickel-base compositions as well as by special alloys of gold, palladium and platinum. Nickel-base alloys provide a wide variety of filler metals to meet the requirements as to mechanical properties and heat and corrosion resistance qualities. Alloying elements such as silicon, boron, phosphorus and copper are added to the nickel in order to lower its melting point and to promote wettability. Chromium enhances the oxidation resistance, while other elements are increasing the mechanical properties of the joint.

The presence of such reactive metals as Ta, Ti, and Nb, in most of the Ni-based superalloys leads to the formation of oxides in these alloys which are extremely difficult to reduce and wet only in a vacuum or in a dry hydrogen atmosphere. Brazing of these alloys must therefore be carried out in a vacuum better than $\sim 10^{-5}$ mm

Hg and at temperatures higher than 1075 C (1967 F). Unfortunately, high diffusion rates at that temperature often cause grain growth in the base metal and a consequent drastic reduction of mechanical properties. Furthermore, the aggressive effects of the filler metal may be severe at these high temperatures.

Ternary Alloys

The brazing filler metals most commonly used in high-vacuum brazing processes of nickel-base alloys are ternary alloys of the type Ni-A-B (A and B being alloying elements). Equilibrium diagrams of most of these ternary systems are only partly known and, therefore, neither the primary nor the secondary phases which appear after brazing can, as a rule, be easily predicted.

The BNi5 filler metal used in the present investigation is basically a ternary alloy Ni-Cr-Si (< 0.1 wt-% C, 70 wt-% Ni, 20 wt-% Cr, 10 wt-% Si). According to data available from the literature[1] for the composition 70% Ni, 20% Cr and 10% Si, the solidus temperature is approximately 1100 C (2012 F), which decreases by at least 30 C (54 F) in the presence of carbon. The phases that may be expected in the brazed joint are Ni_5Si_2, Ni_4Cr_2Si, $Ni_3Cr_3Si_2$ and an FCC solid solution of Ni-Cr-Si.

Weldability of Inconel 718 Alloy

A property, apparently unique to Inconel 718 alloy among the superalloys, is the outstanding weldability of the material in either the age-hardened or the annealed condition. This superior weldability is the result of strengthening by the precipitation of a Ni_3(Mo, Al, Ti) γ' phase rather than by the usual Ni_3 (Ti, Al) γ' precipitation. The precipitation of Ni_3(Ti, Al) γ' is relatively rapid and temperature-sensitive, bearing within it a potential of crack formation during welding or brazing.

The Ni_3(Nb, Al, Ti) precipitate in Inconel 718 responds very sluggishly to thermal cycling, thereby reducing the precipitation hardening which usually occurs during temperature changes in welding or brazing processes. This slow response to thermal cycling, and the additional fact that titanium and aluminum oxides do not form impenetrable barriers, make the Inconel 718 nickel-base alloy a prime candidate for joining by brazing techniques.

High-temperature vacuum brazing, similar to other joining techniques, does not guarantee a structurally perfect joint, even under the most painstaking and closely controlled conditions of the brazing operations. As previously mentioned, the formation of oxides, wetting problems, temperature changes, etc., may lead to the development of local discontinuities in the structure. Although these flaws may play a minor role as far as the conventional static strength of the brazed joint is concerned, they assume a major importance in achieving the state of crack instability.

Table 1—Chemical Composition of the RGT 601 (Inconel 718) Nickel-Base Alloy and the Brazing Filler Metal BNi5, %

	RGT 601	BNi5
C	0.05	0.1
Cr	18.5	20.0
Ni	53.0	70.0
Mo	3.0	–
Fe	Balance	–
Al	0.6	–
Ti	0.8	–
Nb/Ta	5.3	–
Si	–	10.0

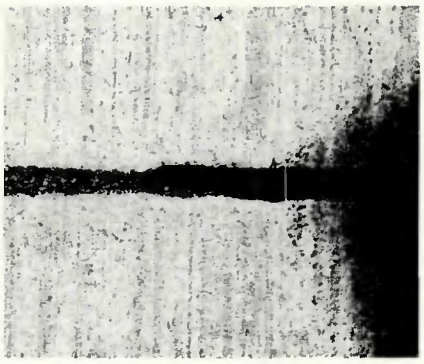

Fig. 1—Notch specimens deepened by using steel wire. ×50 (reduced 34% on reproduction)

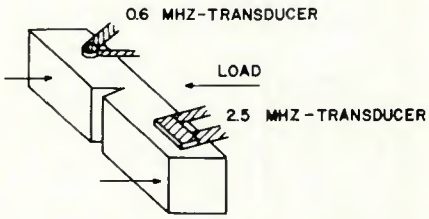

Fig. 2—The LSH crystals (transducers) attached to the specimen (schematic presentation)

Crack Toughness/Propagation

Most measurements of crack toughness are conducted in static or quasi-static conditions which do not always represent the real situation in the state of crack instability. Even in structures subjected to static loading, high strain rates are liable to occur in microscopic regions in the immediate vicinity of structural discontinuities. Dynamic rather than static characterization of crack instability is, therefore, a better choice for fracture-safe design, especially for strain-rate sensitive materials.

Measuring dynamic crack propagation in unstable conditions was once a very laborious procedure as regards both the preparation of specimens and the testing method employed. When, however, instrumentation was added to the impact testers, new ways were opened for evaluating the dynamic response of a wide range of materials.

Fracture toughness measurements performed in the state of plane strain in either static or dynamic conditions lead to the establishment of toughness parameters which characterize the crack instability. They do not supply any information about the microscopic crack growth mechanisms. Some information about the mechanisms can be obtained from "post mortem" fractographic studies of the fractured surface by using scanning and transmission electron microscopy. However, very seldom do these techniques supply information about the chronology or characteristic features of the individual cracking events.

In order to develop a better understanding of the crack propagation process, *in situ* measurements are desirable and, indeed, necessary. Acoustic emission, which is the spontaneous emission of sonic pulses accompanying events such as deformation, crack propagation, etc. in solid materials, has the potential of detecting individual crack events. Acoustic emissions, which are stress waves that carry part of the elastic energy released during the deformation or crack propagation, have an extremely low amplitude, which makes them sometimes difficult to detect and to study.

One of the first investigations on the combined use of acoustic emissions and fracture mechanics was reported by Jones and Brown.[2] Since then great improvements have been made in the measuring technique and relevant theoretical models.[3-6]

Scope of Present Investigations

In the present paper, the results of investigations of crack toughness of brazed joints of Inconel 718 at different strain rates are reported. The results are compared with those obtained on specimens made of the base material. In the static and quasi-dynamic investigations, acoustic emissions were recorded as a function of time simultaneously with load and crack opening displacement.

Materials, Heat Treatments, and Experimental Procedure

The materials used in this investigation were a nickel-base alloy Inconel

718, which was supplied by the Rochling Company and which bears the commercial designation RGT 601 and the brazing filler metal BNi5. The chemical compositions are given in Table 1.

Brazing was carried out in high vacuum ($\sim 10^{-5}$ torr) and at temperatures of 1180–1190 C (2156–2174 F). Brazing time was approximately 10 min. The specimens, cut parallel with the rolling direction, were, after brazing, cooled to room temperature and afterwards heat treated. Several sequences of heat treatments were introduced and studied. After each heat treatment the brazed joint and the base metal were subjected to metallographic investigations, as a result of which the following heat treatments were chosen:

1. Annealing at 1100 C (2012 F) for 10 hours (h). The annealing process is a combination of the homogenization of the brazed joint and a solution treatment.
2. Air cooling.
3. Aging for 8 h at 720 C (1328 F), furnace cooling to 620 C (1148 F), and aging for a further 8 h.
4. Air cooling.

According to the present studies this sequence of heat treatments leads to an improved distribution of the brittle phases in the brazing joint and a relatively small grain growth in the base metal. The static and quasi-dynamic fracture toughness specimens were tested in three-point bending on a 6-ton (5443 kg) Schenk's hydropulse testing machine. Dynamic (impact) fracture toughness experiments were conducted on an instrumented Tinius Olsen impact machine of 30 kgm maximum capacity.

Specimens for measuring parameters describing the crack instability (fracture toughness) are generally fatigue precracked, but this procedure was abandoned after a few attempts of fatigue precracking of the brazed joints had been made, since fatigue crack propagation, even in side-grooved specimens, could not be controlled. Instead of fatigue precracking a wire-sharpening procedure was, therefore, used. A notched specimen was sharpened by the repeated sawing motion of a steel wire ($\sim 80\ \mu m$ dia) smeared with a diamond paste (7 μm). An example is shown in Fig. 1. The same procedure for specimen preparation was used with the base material in order to facilitate the comparison of experimental results obtained on both types of specimens, viz., base material and brazed joint.

All experiments were carried out at room temperature.

The fracture toughness was calculated from the equation used in fracture mechanics for three-point bending:[7]

$$K_{Ic}\ (K_{Id}) = \frac{6YMa^{1/2}}{BW^2} \qquad (1)$$

where: $Y = 1.93 - 3.07\left(\frac{a}{W}\right) + 14.53\left(\frac{a}{W}\right)^2 - 25.11\left(\frac{a}{W}\right)^3 + 25.8\left(\frac{a}{W}\right)^4$

Also: M—bending moment; a—crack length; B—specimen thickness; W—specimen width.

In order to monitor *in situ* all events at the crack tip which may be relevant to the processes of crack formation and crack propagation, acoustic emission was used; but the customary transducers were unsuitable for the purpose. They were too big either to be fixed on the relatively small impact specimen or to be attached to the relevant area of the testing machine.

Small, specially cut LSH crystals were, therefore, used as transducers for acoustic emissions, viz., a circular 0.6 MHz transducer of about 3 mm (0.12 in.) diameter and a rectangular 2.5 MHz transducer, 6 × 10 mm (0.24 × 0.39 in.). Both transducers were 1 mm (0.04 in.) thick and were attached to the impact specimen as shown in Fig. 2. The emitted signals were first passed through a preamplifier, then adequately filtered and finally amplified by the main amplifier. From there the signals were passed to a totalizer or to an oscilloscope and transient recorder. The block diagram in Fig. 3 outlines the experimental setup.

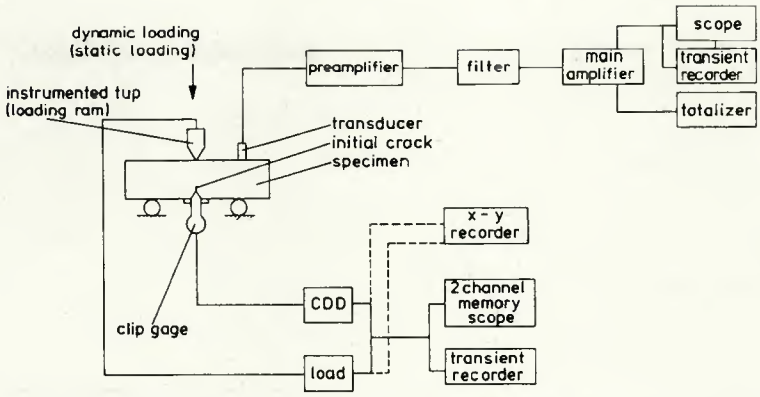

Fig. 3—Block diagram of the experimental setup. Solid lines—dynamic loading; dashed line—static loading

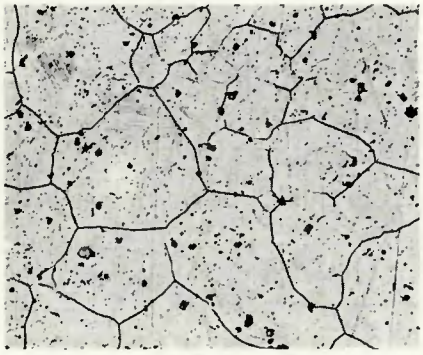

Fig. 4—Equiaxial grain structure of the annealed Inconel 718 nickel-base alloy. ×200 (reduced 34% on reproduction)

Fig. 5—Structure of the brazed joint after brazing. Dendrites and other particles are heterogeneously distributed over the matrix. ×400 (reduced 50% on reproduction)

Fig. 6—Structure of the brazed joint after the solution treatment and two-stage age hardening. Part of the hard phases were dissolved by the matrix. ×400 (reduced 50% on reproduction)

Fig. 7—Grain growth in the base material as a result of the heat treatment. ×200 (reduced 50% on reproduction)

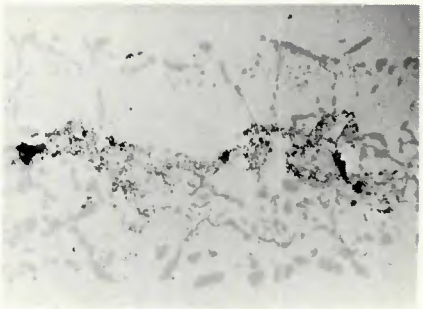

Fig. 8—Porosity in the brazed joint. ×400 (reduced 50% reproduction)

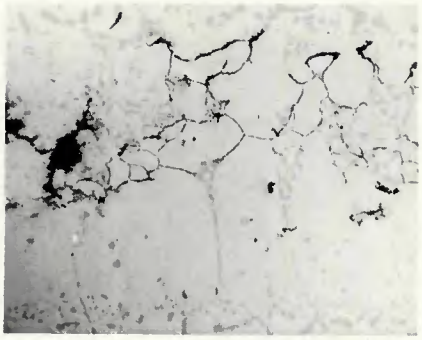

Fig. 9—Cracks along grain boundaries in the brazed joint. ×400 (reduced 50% on reproduction)

Results and Discussion

Metallographic Examinations

The main purpose of the metallographic studies was to establish structural changes which occur in the brazed joint and in the base material during brazing and the prolonged heat treatments (solution treatment and hardening).

In the brazed joint, in the first stage, the main interest was directed towards the formation of hard phases (presumably silicides) during the brazing process, their morphology and distribution. In the second stage, changes in the morphology and the distribution of the hard phases as a result of the heat treatments were tracked. In the base material the influence of the heat treatments on the grain growth was studied. All metallographic investigations presented in this paper were limited to optical microscopy.

Figure 4 shows the annealed equiaxial grain structure of the FCC matrix with rather uniform distribution of an unidentified phase (phases?) of the annealed Inconel 718 alloy in the as-delivered conditions. The austenitic grain size is 4 according to ASTM.

Table 2—"Static" Tensile Properties of the Base Material and the Brazed Joint

Type of specimen[a]	$YP_{0.2}$,[b] kg/mm²	UTS,[c] kg/mm²
I	33.0	79.5
II	94.0	122.0
III	28.0	74.0
IV	74.0	104.0
V	61.0	70.5

[a] For a description of the different types of specimens see text.
[b] YP—yield point (or stress). Two specimens of each type were tested, the values given being an average of both tests. The yield stress (0.2% offset) of the brazed joint is an approximate value. The width of the brazed joint is ≃100 μm but the 0.2% effect was measured by means of strain gauges 300 μm long.
[c] UTS—ultimate tensile strength. The values given are each the average of two tests.

Figure 5 shows the structure of the brazed joint after brazing. Dendrites and other particles of primary or secondary phases (silicides? carbides?) distinguished by different morphologies are heterogeneously distributed in the matrix. Both the heterogeneity and the characteristic morphology can be explained by a combination of solidification conditions which are controlled by the directions of the heat transfer—and by the mechanism of precipitation of the different phases in the brazed joint. The "hard" phases were not identified, but from their morphology and microhardness test results, it can be concluded that more than one phase must be present.

The microhardness tests carried out across the brazing joint point to the presence of at least three different phases of different microhardness. The dendritic structure has a microhardness of 1000 to 1200 DPH; the flake-like precipitates, 700 to 900 DPH, and the matrix of the joint 450 to 600 DPH. The microhardness of the base material in the region of the brazed joint was found to be between 350 DPH and 450 DPH.

Figure 6 shows the structure of the brazed joint after the solution treatment at 1100 C (2012 F) for 10 h and the two-stage age hardening, at 720 C (1328 F) and at 620 C (1148 F), for 8 h at each stage. Part of the hard phases were dissolved by the matrix, but both the dendritic structure and the flake-like precipitates were still discernible. Generally speaking, the morphology of the brazed joint after the heat treatments described above is much more favorable from the point of view of the

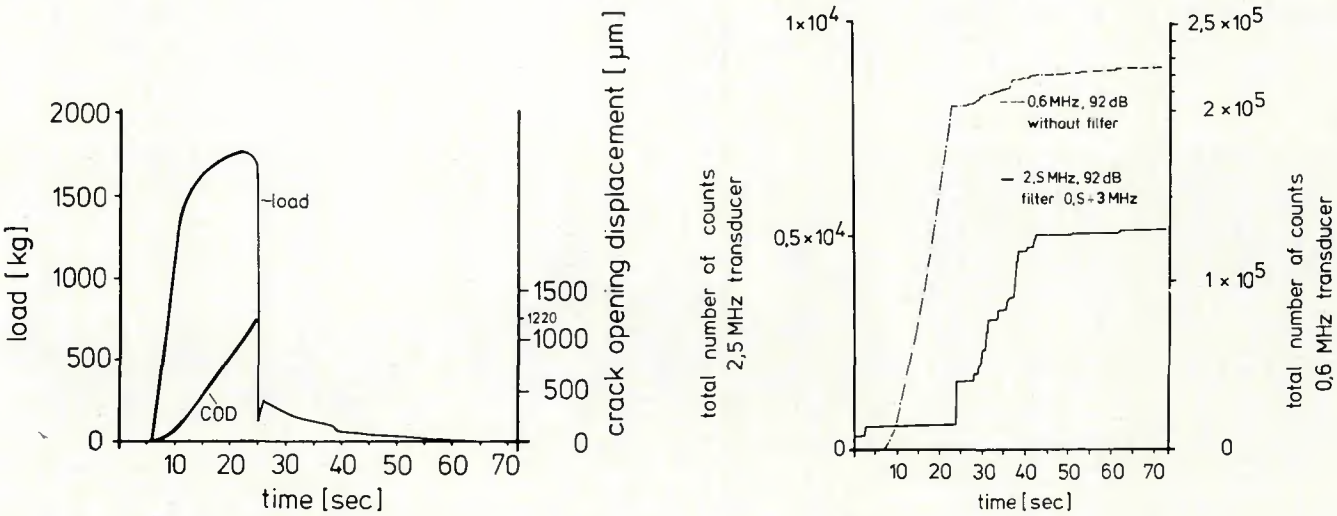

Fig. 10—Load, crack opening displacement and related acoustic emissions as functions of time. Low carbon steel bent specimen tested at a strain rate of $\dot{\varepsilon} \sim 10^{-3} s^{-1}$

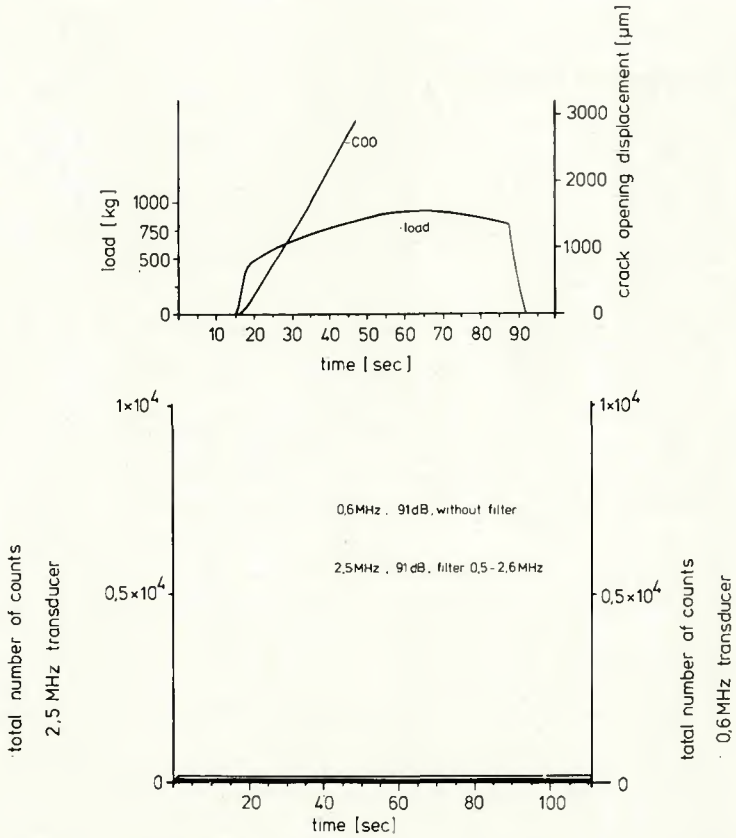

Fig. 11—Precracked bending specimen of the base material tested in static loading ($\dot{\varepsilon} \sim 10^{-3} s^{-1}$). No acoustic emissions were recorded

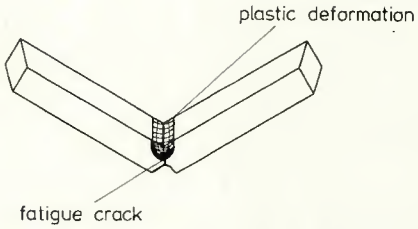

Fig. 12—Schematic presentation of the volume of the material plastically deformed during bending after the state of general yielding had been reached

mechanical behavior. The microhardness tests carried out across the brazed joint showed that the hardness of different phases had decreased considerably, pointing to some metallurgical, diffusion-controlled changes.

The prolonged solution treatment (homogenization) at 1100 C (2012 F) causes some grain growth in the base material 3 according to ASTM (see Fig. 7). However, this grain growth affected the mechanical properties of the base material to only a limited extent. According to the results of the present study, this was the best compromise that could be reached between the improvement of the properties of the brazed joint and the worsening of those of the base material.

As mentioned in the Introduction, brazed joints are not completely free from flaws and defects introduced by the brazing process. Figures 8 and 9 show two typical flaws: porosity (Fig. 8) and cracking along grain boundaries (Fig. 9).

All the results presented above are based on metallographic studies at the low magnifications available in optical microscopy. It is obvious that they are insufficient and that a more detailed study on the level of electron microscopy is required. Such an investigation is important, since the presence of different hard phases and their morphology can be controlling factors in crack formation and propagation, but this was beyond the scope of the present investigation.

Tensile Properties

It was already mentioned that in a system combining two diametrically different structures (brazed joint and base material), a compromise heat treatment must be given which will guarantee an improvement in the mechanical behavior of the brazed joint without causing any drastic worsening of the properties of the base material.

The main problem is the grain growth in the base material during the prolonged solution treatment (homogenization) at 1100 (2012 F).

The results of the pertinent investigations and the suggested sequence of heat treatments after the brazing process are given above. In this section, results of tensile tests carried out on specimens that had been subjected to different heat treatments are reported. The main purposes of the tensile tests were to define to what extent the grain coarsening resulting from the prolonged solution treatment at 1100 C (2012 F) affected the mechanical properties of the Inconel 718 alloy and to compare properties of the base material with the brazed joint. Five series of tensile specimens were prepared from the Inconel 718 alloy and the brazed joint:

1. As supplied (solution treated for 1 h at 955 C, i.e., 1751 F)—base material.
2. As supplied (solution treated for 1 h at 955 C (1751 F), two-stage age hardening at 720 and 620 C (1328 and 1148 F) for 8 h in each stage)—base material
3. As supplied, homogenized for 10 h at 1100 C (2012 F)—base material.
4. After delivery, homogenized for 10 h at 1100 C (2012 F), two-stage hardening at 720 C and 620 C (1328 and 1148 F) for 2 h in each stage—base material.
5. Brazed joint after the full heat treatment.

The results of these tests are presented in Table 2.

As can be seen from these results, the grain growth in the base material caused by homogenization for 10 h at 1100 C (1982 F) leads to a certain decrease in tensile strength properties. The yield strength drops by ~10% (specimens "I" and "III" in Table 2). The decrease in tensile properties is even more pronounced after the final age hardening treatment. The yield strength decreases by ≃20% and the ultimate tensile strength by ≃15% (specimens "II" and "IV" in Table 2).

Comparing the tensile properties of the brazed joint with those of the base material, it can be seen (from Table 2) that the tensile properties of the brazed joint are lower than those of the base material. This is not unexpected, considering the presence of the hard phases and the substantial differences in the chemical composition. The approximate yield strength of the brazed joint is by ~20% lower than that of the base material, while the ultimate tensile strength is lower by ~30% (specimens "IV" and "V" in Table 2).

Acoustic Emission Measurements

Acoustic emission arises from the energy released when a solid material undergoes plastic deformation and

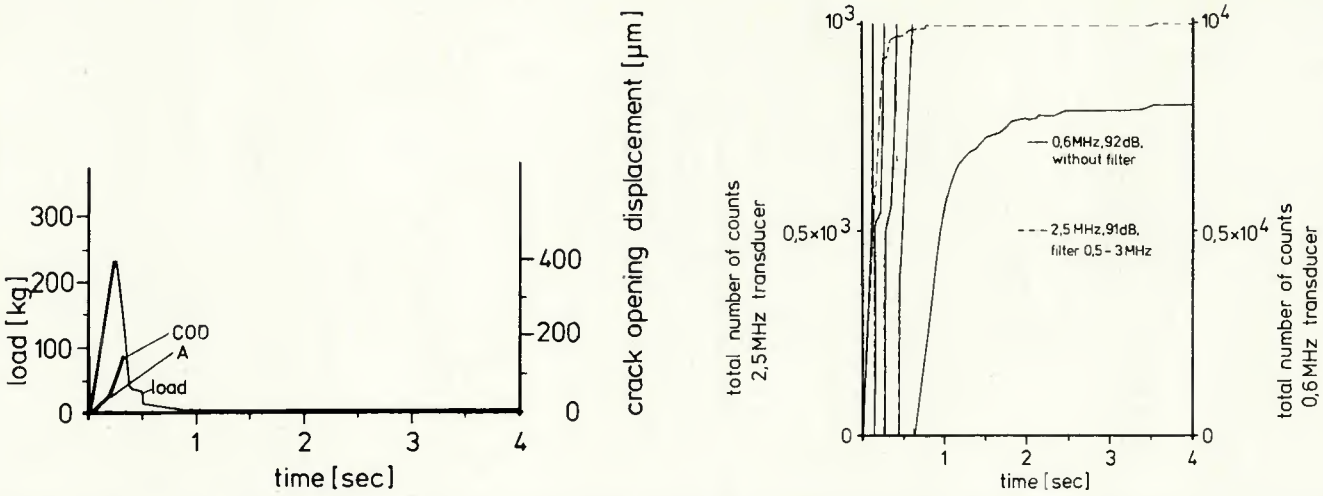

Fig 13—Load, crack opening displacement and related acoustic emissions as functions of time. Brazed specimens tested at strain rate $\dot{\epsilon} \sim 10^{-1} s^{-1}$

propagation of cracks. Part of this energy is converted into elastic waves which propagate through the material and are detectable at its surface by highly sensitive sensors (transducers).

In the present investigation LSH crystals served as transducers with frequencies of 0.6 MHz and 2.5 MHz. The reason for using two types of sensors was that the low frequency transducers are more sensitive for registering acoustic events associated with plastic deformation, while the higher frequency transducers are more sensitive for registering acoustic events associated with crack formation and propagation,[8] usually indicated by discontinuous changes in the total number of counts as a function of time, as can be seen in Fig. 10.

The acoustic emissions were recorded as a function of time simultaneously with load and crack opening displacement (COD). The latter was measured with a double cantilever beam clip gauge. This type of recording permitted relating the COD and load to the acoustic emissions at any time. Already in the first experiments on the presawed (precracked) specimens of the base material, difficulties in recording acoustic emissions were encountered. In all specimens tested in static and quasi-dynamic loadings, no acoustic emissions could be detected, while changes in COD and load were monitored easily—Fig. 11.

This behavior can probably be explained as follows: The Inconel 718 superalloy is a nickel-base alloy characterized by an FCC structure. Most of the grown-in dislocations in this structure are mobile, and their motion begins with the onset of the load. While it is extremely difficult to monitor acoustic emissions caused by the motion of slowly moving single dislocations, it would be reasonable to expect that in later stages of deformation, when the total number of moving dislocations is higher, acoustic signals should be monitored more easily. This is, however, also dependent on the velocity of the moving dislocations and the volume of the deformed material. Since the specimens were tested at relatively slow strain rates in bending, and only small volumes of the material were deformed (Fig. 12), the acoustic emissions were probably not sufficiently intensive, even after the state of general yielding had been reached, to be monitored by the sensors used—Fig. 11.

The fracture process of the base material bent at low strain rates is a slow process of shear accompanied by a probably rather low intensity of acoustic emissions. Consequently, even in the stage of fracture, no acoustic signals could be monitored.

In order to check the explanation given above, low carbon steel specimens having the same geometry were tested in identical loading conditions. The acoustic emissions were recorded, as can be seen in Fig. 10, when the material reached the state of yielding.

The difference in behavior as shown by the emitted acoustic signals can be attributed to the structural differences of both materials. The low carbon steel has a BCC structure, in which most of the grown-in dislocations are immobile, pinned down by impurity atoms. Only when the yield stress is reached does a rapid motion and multiplication of dislocations occur, resulting in intense acoustic emission even from a relatively small deformed volume.

In the brazed joint the situation is completely different. The strengthening effect of the hard phases present in the brazed joint cause the plastic deformation to occur under constraint

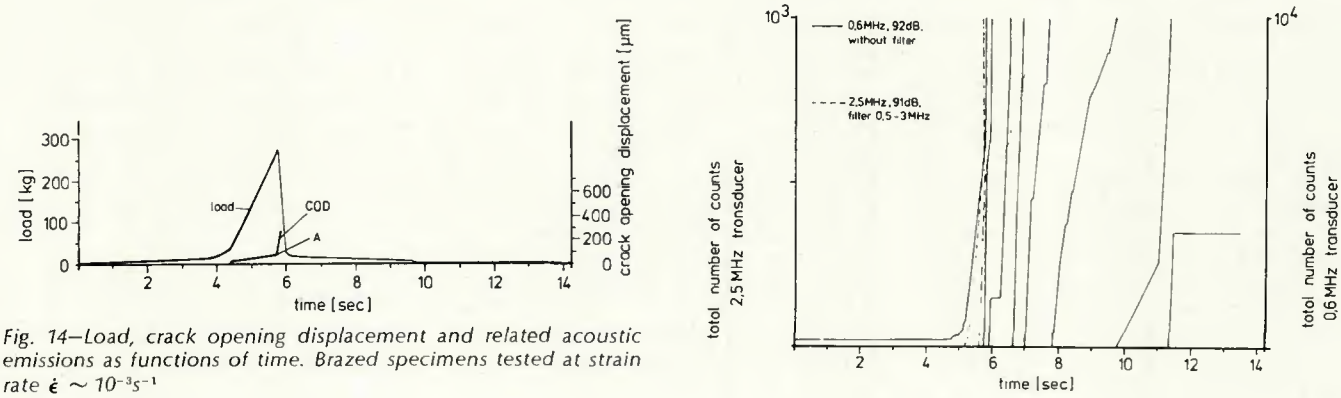

Fig. 14—Load, crack opening displacement and related acoustic emissions as functions of time. Brazed specimens tested at strain rate $\dot{\epsilon} \sim 10^{-3} s^{-1}$

conditions. The motion of dislocations is comparatively rapid, and the emission of acoustic signals is consequently intense. Furthermore, in the early stages of loading, discontinuous changes in the total number of counts could be observed, especially in the specimens loaded at higher strain rates, pointing to the formation and propagation of cracks—Fig. 13.

The crack formation and propagation in the quasi-dynamic specimens tested was so intense that sudden changes in the COD could be observed before the maximum load had been reached—Fig. 13. In the specimens loaded at lower strain rates (Fig. 14), the discontinuous changes were observed only after the maximum load had been reached.

From the results presented in this section, the following conclusions may be drawn concerning the behavior of the brazed joint under loading conditions:

1. First cracks, presumably of the brittle particles, are formed in early stages of loading, well before the load reaches its maximum value.
2. The higher the strain rate, the earlier the beginning of cracking.
3. Cracks appeared on the acoustic emissions vs. time curve before any changes could be observed on the COD-time curve; only when the cracks have propagated substantially, does the COD curve show a discontinuous change in slope, dependent on the strain rate.

At low strain rates this discontinuous change in the slope of the COD-time curve appears immediately after the maximum load has been reached, while at the higher strain rates the slope changes before the maximum load is reached.

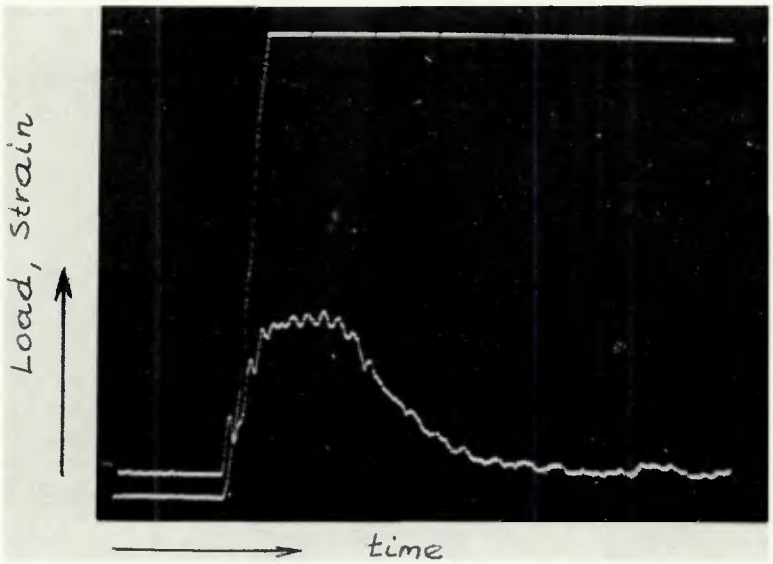

Fig. 15—Strain vs. time and load vs. time curves obtained on a specimen made of base material. Load scale: 1000 kg/div.; strain scale: 0.003/div.; time scale: 500 s/div.

Static and Dynamic Crack Toughness

The crack toughness measurements at strain rates $\epsilon \sim 10^{-3} s^{-1}$ and $\epsilon \sim 10^{-1} s^{-1}$ were carried out in three-point bending on a hydropulse testing machine. The crack toughness itself was evaluated by means of load (COD) vs. time diagrams shown in Figs. 10, 13 and 14. The crack toughness measurements at $\epsilon \sim 10^{2} s^{-1}$ were made with the instrumented impact machine, while the toughness was determined from the load-time curves recorded during the impact. The procedure for determining the crack toughness was the same regardless of the strain rate at which the specimens were tested. Where fracture occurs before general yielding, the K_{Id} values are obtained using linear fracture mechanics considerations.

The strain rate at each loading condition was obtained from the strain vs. time curve recorded by means of a pair of strain gages glued to both sides of the specimen at the tip of the presawed notch and taken simultaneously with the load vs. time curve. Figure 15 shows both curves as recorded on the screen of an oscilloscope during impact loading.

For specimens in which the general yielding occurred before the fracture (maximum) load had been reached, the crack toughness values were calculated by the "equivalent energy method."[9] This method postulates that in a specimen thick enough to avoid general yielding prior to fracture, the amount of energy necessary to reach the maximum (fracture) load is equivalent to the energy required if general yielding sets in before fracture.

Figure 16 shows the experimental results of crack toughness obtained on the specimens of the base material tested at room temperature at different strain rates. The series of specimens in the heat treatment conditions (II) and (IV) were investigated.

Figure 15 shows a typical load-time diagram obtained by impact tests on specimens of the base material. The non-linear dependence between load and time is characteristic for specimens in which fracture occurs after general yielding. The first peak seen in the initial stages of loading is the inertia peak.[10]

As can be seen from the results presented in Fig. 16, the prolonged homogenization process at 1100 C, i.e., 2012 F, [heat treatment (IV)] results in a decrease in the crack toughness of the base material in comparison with

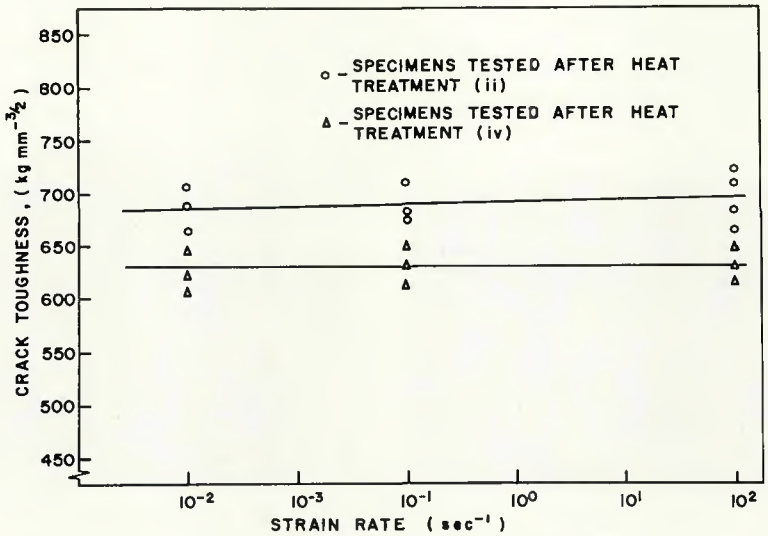

Fig. 16—Crack toughness results, evaluated by the equivalent energy method, vs. strain rate. Base material

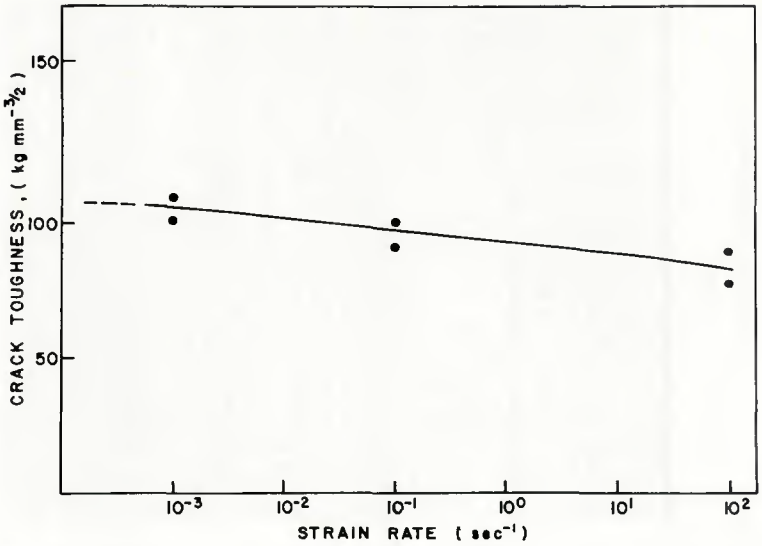

Fig. 17—Crack toughness results, evaluated according to LEFM, vs. strain rate. Brazed joints

results obtained from the same specimens homogenized (solution treated) at only 955 C, i.e., 1751 F [heat treatment (II)]. The decrease amounts to ~10% and may be attributed to grain growth. The crack toughness is for all practical purposes independent of the strain rate. The latest results were not unexpected because of the FCC structure characteristic for the Inconel 718 nickel-base alloy.

Figure 17 presents crack toughness results obtained at room temperature from specimens of the brazed joint tested in heat treatment conditions described in point (V).

In contrast to the non-linear dependence between the load and time observed in the specimens of the base material, the time-load dependence in the specimens of the brazed joint was linear until fracture at all strain rates applied—Figs. 13, 14 and 18. The crack toughness was, therefore, determined by using linear elastic fracture mechanics (LEFM) considerations.

The load-time curve shown in Fig. 18 is not exactly linear. The first peak is the inertia peak, while the two other discontinuities can probably be attributed to crack formation in the brittle phases, propagation of which was arrested for a very short time by the surrounding ductile matrix, until, in fact, the load reached the level characteristic for crack instability. This behavior was observed during acoustic emission measurements, carried out at lower strain rates, which confirmed that some formation and propagation of cracks had been reached well before the maximum load was reached. Unfortunately, because of objective difficulties, no acoustic emission measurements could be conducted during the impact test.

Macroscopically, the mechanical behavior of the brazed joint constitutes typical brittle behavior as displayed by the low crack toughness. Comparing the results presented in Figs. 16 and 17, it can be seen that the crack toughness of the brazed joint is much lower than that of the base material. The drop is relatively drastic and, for heat treatment (IV), amounts to an average of ~80%.

Another difference observed is some dependence of the crack toughness of the brazed joint on the strain rate—Fig. 17. This is probably due to some strain rate sensitivity of the brittle phases present in the brazed joint. The improvement in the crack toughness of the brazed joint must be associated with a process of preventing the appearance of brittle phases, which is probably impossible to achieve; however, it seems that by technological means the morphology of the brittle phases can be considerably improved. This problem must be further investigated.

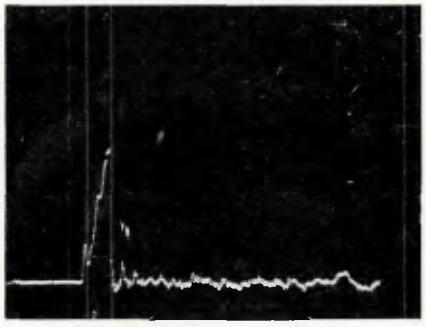

Fig. 18—Oscilloscope traces of the load-time dependence in specimen of the brazed joint tested at strain rate $10^2 s^{-1}$. Load scale: 125 kg/div.; time scale 50 μs/div.

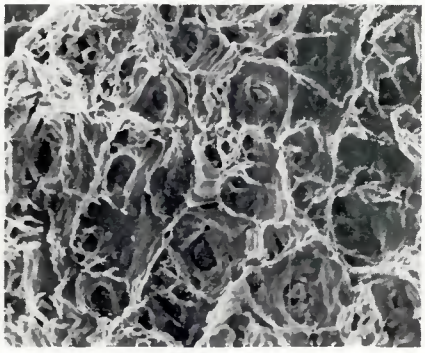

Fig. 19—Oval dimples (tear dimples) and some equiaxed dimples characteristic of the fracture surface of the base material. ×600 (reduced 34% on reproduction)

Fractographic Examination

The fracture topography very often reflects the manner in which the fracture has developed. Fractographic studies "post mortem" may, therefore, cast enough light on pertinent features to permit the micromechanisms which led to the final failure to be understood.

In the present study the main purpose of the fractographic examinations was to establish differences between the appearances of the fractures in broken specimens of the base material and of the brazed joint. Another purpose was to explain the drastic differences in crack toughness values which were established experimentally and are summarized in the previous section.

The fractures of the specimens of the base material were found to be almost identical for all strain rates applied in this investigation.

Figure 19 shows a scanning fractograph of the fracture surface of a specimen broken at a strain rate of ~$10^2 s^{-1}$ (impact test).

The fracture surface, formed primarily by the tearing mode of microvoid coalescence, shows oval dimples (tear dimples) uniformly distributed. In addition, some equiaxed dimples (normal dimpled rupture) could be observed. This type of fracture requires a relatively high input of energy. In contrast, the fracture surface of the brazed joint testifies to a low energy fracture. Figure 20 shows the fractograph of a specimen broken at the strain rate mentioned before. The fracture surface consists primarily of cleavage facets; but in the region where dendrites are present it becomes a "herringbone" pattern.

Figure 21 shows small cracks which formed probably before the load had reached its maximum value; their propagation was in all likelihood arrested by the surrounding ductile matrix.

From the results of the fractographic investigations presented here, it can be seen that there is a clear difference

in fracture appearance between the specimens made of the base material and those made of the brazed joint. The mechanisms of crack propagation in the base metal are dominated by microscopic plastic deformation processes. This type of fracture requires a high energy input. In contrast, the fracture of the brazed joint is predominantly a brittle, low energy fracture dominated by cleavage or quasi-cleavage mechanisms.

Summary

The crack toughness of brazed joints of Inconel 718 nickel-base alloy was investigated at different strain rates. The brazing filler metal used was BNi5. The results were compared with those obtained on specimens made of the base material. In order to achieve a desirable distribution of the brittle phases in the brazed joint and to avoid intensive grain growth in the base material, the following sequence of heat treatments was chosen after the brazing process: homogenization at 1100 C (2012 F) for 10 h, air cooling, aging for 8 h at 720 C (1328 F), furnace cooling to 620 C (1148 F), and aging for a further 8 h, followed by air cooling.

Tests for determining static tensile properties, carried out on five series of specimens, have shown that the homogenization treatment at 1100 C (2012 F) for 10 h leads to a certain reduction in tensile strength. The yield stress drops by ~15% and the ultimate tensile stress by ~10%. The decrease in tensile properties is even more pronounced after the final age hardening treatment. The yield stress decreases by ~20% and the ultimate tensile strength by ~15%. The tensile properties of the brazed joint are lower than those of the base material. This is due primarily to the presence of hard phases and to substantial differences in the chemical compositions. The yield stress of the brazed joint is lower by ~20% than that of the base material, while the ultimate tensile stress is lower by ~30%.

In the static and the quasi-dynamic crack toughness investigations, acoustic emissions were recorded as a function of time simultaneously with load and crack opening displacement. In all specimens made of the base material and tested in static and quasi-dynamic loading, no acoustic emissions could be detected. This was explained by the fact that Inconel 718 has an FCC structure, in which most of the grown-in dislocations are mobile and their motion begins with the onset of the load.

Since the specimens were tested at relatively low strain rates in bending—in which only a small volume of

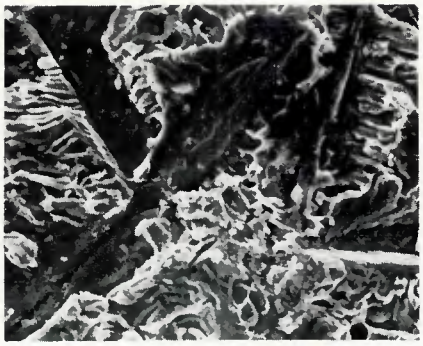

Fig. 20—Cleavage facets, and herringbone patterns in regions where dendrites are present. ×600 (reduced 34% on reproduction)

Fig 21—Small cracks formed probably before the load had reached its maximum value. Specimen tested at $\epsilon \sim 10^{2} s^{-1}$. ×3000 (reduced 34% on reproduction)

the material is deformed—the acoustic emissions associated with the plastic deformation (dislocation motion) were not sufficiently intensive for monitoring by the sensors used. The fracture of the base material was completely controlled by the plastic deformation, as confirmed by the fractographic studies; thus, even during the process of fracture, it was impossible to record acoustic emissions. In brazed joints the plastic deformation occurs under constraint conditions, the dislocation motion is comparatively rapid, and emissions of acoustic signals are consequently intense. In addition to acoustic emissions associated with plastic deformation, emissions resulting from crack formation and propagation in the brittle phases could be easily recorded.

In the base material fracture occurred after general yielding, and the crack toughness values were therefore calculated by the "equivalent energy method." The prolonged homogenization at 1100 C (2012 F) was found to result in a decrease in the crack toughness of the base material by ~10% as compared with the crack toughness results obtained from the specimens that had been solution-treated at 955 C (1751 F).

In contrast to the base material, fractures of the brazed joints were of a typical brittle character, as reflected by the linear dependence between load and time (until fracture) and confirmed by the fractographic investigations. The crack toughness at the brazed joint is much lower than that of the base material. The drop is relatively sharp and amounts to an average of ~80%. Another difference observed is a certain dependence of the crack toughness of the brazed joint on the strain rate, an effect which was not observed in the base material.

Acknowledgment

The authors are greatly indebted to Min-Rat. Dipl. Ing. W. Simmler and to Dipl. Ing. P. Balzerowiak (German Ministry of Defence) for their personal interest and the fruitful suggestions during the performance of this research. The financial support of the German Ministry of Defence is gratefully appreciated. Special appreciation is extended to Dr. Ing. A. Crostack for his help, critical discussions, and encouragement during all stages of the performance of this research. The assistance of Mr. Bainke, Mr. Knipschild and Mrs. Edel as well as all colleagues at the University of Dortmund is all appreciated.

References

1. Gray, I., and Miller, G. P., *Jour. Inst. Met.* 93, (1964), p. 315.
2. Brown, W.F., and Jones, M.H., "Acoustic Detection of Crack Initiation in Sharply Notched Specimens," Mater. Res. Stand. 4, (1964), p 120.
3. Schofield, B.H., "Research on the Sources and Characteristics of Acoustic Emission," *Acoustic Emission ASTM STP 505*, (1971), p 11.
4. Palmer, I.G., Brindley, B.J., and Harrison, R.P., "The Relationship Between Acoustic Emission and Crack Opening Displacement Measurements," *Mat. Science Eng.*, 14, (1974), p. 3.
5. Tetelman, A.S., "Acoustic Emission and Fracture Mechanics Testing of Metals and Composites," DAH-04-68-C-0008 Report U.S. Army Res. Office, July, 1972.
6. Eisenblatter, J., Jax, P., and Schwalbe, H.J., "A Survey of Acoustic Emission Research in Europe and Investigations Conducted at Battelle Frankfurt," The Second Acoustic Emission Symposium, Tokyo, Japan (1974).
7. Brown, W.F., and Strawley, E.J., "Plane Strain Crack Toughness Testing of High Strength Metallic Materials," ASTM, STP 410 (1966).
8. Crostack, H.A., Private Communication.
9. Witt, F.J., *Proc. of Fourth National Symposium on Fracture Mechanics*, Pittsburgh, Pa. Aug. 1970, 24.
10. Ireland, D. R., "Procedures and Problems Associated with Reliable Control of the Instrumented Impact Test," *Instrumented Impact Testing*, ASTM STP 563, 1974, p. 3.